Article

Spermine Oxidase-Substrate Electrostatic Interactions: The Modulation of Enzyme Function by Neighboring Colloidal ɣ-Fe_2O_3

Graziano Rilievo , Massimiliano Magro , Federica Tonolo , Alessandro Cecconello , Lavinia Rutigliano , Aura Cencini , Simone Molinari , Maria Luisa Di Paolo , Cristian Fiorucci , Marianna Nicoletta Rossi , Manuela Cervelli * , Fabio Vianello

Posted Date: 9 November 2023

doi: 10.20944/preprints202311.0583.v1

Keywords: Nanoenzyme; Spermine oxidase; Enzyme activity; Electrostatic interactions; Ionic strength; Enzyme nano-immobilization

Article

Spermine Oxidase-Substrate Electrostatic Interactions: The Modulation of Enzyme Function by Neighboring Colloidal ɣ-Fe_2O_3

Graziano Rilievo [1], Massimiliano Magro [1], Federica Tonolo [1], Alessandro Cecconello [1], Lavinia Rutigliano [2], Aura Cencini [1], Simone Molinari [3], Maria L. Di Paolo [4], Cristian Fiorucci [5], Marianna Nicoletta Rossi [5], Manuela Cervelli [5,*] and Fabio Vianello [1,6]

[1] Department of Comparative Biomedicine and Food Science, University of Padua, Viale dell'Università 16, 35020 Legnaro, Italy
[2] Department of Molecular medicine, Sapienza University of Rome, Laboratory Affiliated to Istituto Pasteur Italia, Fondazione Cenci Bolognetti, Sapienza University of Rome, Viale Regina Elena 291, 00161 Rome, Italy
[3] Department of Geosciences, University of Padua, Via Gradenigo 6, 35131 Padova, Italy
[4] Department of Molecular Medicine, University of Padua, Via G. Colombo 3, 35131 Padova, Italy
[5] Department of Sciences, University of Roma 3, Viale Guglielmo Marconi 446, 00146, Rome, Italy
[6] International Polyamines Foundation 'ETS-ONLUS', Via del Forte Tiburtino 98, 00159 Rome, Italy
* Correspondence: manuela.cervelli@uniroma3.it; Tel.: +39 06 5733 82448.

Abstract: Protein–nanoparticle hybridization can ideally lead to novel biological entities characterized by emerging properties, which can sensibly differ from those of the parent components. Herein, the effect of ionic strength on the biological functions of recombinant, His-tagged spermine oxidase (i.e., SMOX) was studied for the first time. Moreover, SMOX was integrated to colloidal surface active maghemite nanoparticles (SAMNs) by direct self-assembly, leading to a biologically active nano-enzyme (i.e., SAMN@SMOX). The hybrid was subjected to an in-depth chemical-physical characterization highlighting that protein structure was perfectly preserved. The catalytic activity of the nanostructured hybrid (SAMN@SMOX) was assessed by extracting kinetics parameters using spermine as substrate and compared to the soluble enzyme as a function of ionic strength. Results revealed that the catalytic function was dominated by electrostatic interactions and that they were drastically modified upon hybridization with colloidal ɣ-Fe_2O_3. Noteworthy, the affinity of SMOX toward spermine was significantly higher for the nanohybrid at low salinity. The present study supports the vision of using protein–nanoparticle conjugation as a mean for modulating biological functions.

Keywords: nanoenzyme; spermine oxidase; enzyme activity; electrostatic interactions; ionic strength; enzyme nano-immobilization

1. Introduction

Spermine oxidase (here abbreviated as SMOX; EC 1.5.3.16) is a dimeric FAD (flavin adenine dinucleotide)-containing enzyme involved in the polyamine catabolic pathway, oxidizing spermine into spermidine, 3-aminopropanaldehyde, and hydrogen peroxide as reaction products in the presence of oxygen [1]. Besides its importance in regulating polyamines homeostasis in cells, it can represent an attracting option for enzyme therapy. As an example, the ability of generating toxic species [2,3] can be a potential key for circumventing multidrug resistance (MDR) of tumour cells [4]. Indeed, SMOX belongs to a group of enzymes already tested for inducing cytotoxicity in human cancer cells, such as bovine serum amine oxidase (BSAO) [5,6]. Indeed, SMOX activity products, such as reactive oxygen species, H_2O_2, and the 3-aminopropanal aldehyde, are able to evoke cellular damage, leading to several pathologies [7–10].

 doi:10.20944/preprints202311.0583.v1

Unfortunately, the applicability of enzymes as drugs in real-world scenarios is hampered by limitations, such as very low membrane permeability and intrinsic instability [11]. Nanomaterials are currently widely studied as innovative delivery strategy for biomolecules, drugs and enzymes into cells [12], and novel smart nanovehicles are proposed for targeting diseased tissues [13].

In the last decade, the hybridization of nanoparticles and enzymes counted on a plethora of core materials [14] and binding strategies [15]. Although the influence of enzyme immobilization on structure and activity is hardly predictable and can lead, at worst, to protein denaturation and loss of biological function [16], the enhancement of enzyme activity is realistic as well, and seems to depend on the proper protein–nanoparticle combination [17,18]. In this view, a number of examples were proposed for the immobilization of enzymes, leading to increased stability [19], enhanced activity, specificity, and selectivity, compared to soluble enzymes [20].

Overall, protein-nanomaterial interactions are extremely complex and far from being fully comprehended, requiring suitable nanomaterial surfaces for harboring the enzyme, as well as delicate binding methods to avoid the well-known immobilization-related risk of protein denaturation. In the limitless arena of nanomaterials, among the choice of available iron oxide nanomaterials, peculiar superparamagnetic nanoparticles constituted of stoichiometric maghemite (ɣ-Fe_2O_3) emerged as versatile platforms for producing self-assembled and functional nano-bio-conjugates. These nanoparticles, called surface active maghemite nanoparticles (SAMNs), are characterized by high colloidal stability in the absence of any superficial modification or coating derivatization and a unique surface chemistry [13]. This endows SAMNs with the ability to bind proteins in a highly selective way and, most importantly, macromolecules with affinity for SAMNs can readily interact with the nanoparticle surface without dramatic structural alterations [21]. On the other hand, even minimal structural rearrangements occurring upon protein docking on SAMNs can result in a relevant change of the immobilized enzyme catalytic activity [22].

In the present work, by coupling His-tagged SMOX and pristine nanoparticles SAMNs, a catalytically active enzyme–nanoparticle hybrid (SAMN@SMOX) was fabricated and characterized.

Herein, along with the intrinsic features of the nanomaterial core, including superparamagnetism and fluorescence [23], the enzymatic cargo (SMOX) displayed new biological features as a consequence of direct immobilization. SAMN@SMOX hybrid can be ideally exploited for cancer therapy, targeting and accumulating SMOX into neoplastic tissues. Secondly, the SAMN@SMOX hybrid displayed a considerably higher affinity toward its substrate. These differences were attributed to conformational alterations of the enzyme as evidenced by circular dichroism spectroscopy and FTIR and by the zeta potential of the final nanohybrid.

2. Materials and Methods

2.1. Reagents

All reagents were purchased at the highest commercially available purity and were used without further purification. His-tagged (HT) SMOX (mouse spermine oxidase) expressed in Escherichia coli was purified according to [24]. The enzyme (Mr = 68 kDa per monomer, 136 kDa the holoenzyme) was obtained at a concentration of 1.42 μg/μL in 10 mM HEPPS buffer (N-[2-hydroxyethyl]piperazine-N′-[3-propanesulfonic acid]) at pH 8.0, and stored at -20 °C. Surface Active Maghemite Nanoparticles (SAMNs) were produced in-house following a protocol by Magro et al. (2012) [25]. HEPPS buffer, sodium chloride (NaCl), di-thiothreitol (DTT), N,N-dimethyl-aniline (DMA), 4-amino-antipyrine (AMP), horseradish peroxidase type II (HRP, 179 units/mg solid) and spermine (Spm) were purchased from Sigma-Aldrich at high grade purity. A series of Nd-Fe-B magnets (N35, 263–287 kJ/m3 BH, 1170–1210 mT flux density by Power magnet—Germany) was used to magnetically recover the nanoparticles.

2.2. Instrumental Analysis

Protein fluorescence was assessed by a Varian Cary Eclipse Fluorescence Spectrometer (Agilent, CA, USA). The instrument settings were as follows: λ_{ex} 280 nm, λ_{em} 300–500 nm, slit 10nm/20nm,

 doi:10.20944/preprints202311.0583.v1

medium scan rate acquisition (600 nm/min). The volume of the samples was 400 µL in a quartz cuvette. For protein quantification by fluorescence, a calibration curve was built with concentrations ranging from 0 to 200 mg/L in 10 mM HEPPS buffer at pH 8.0 (Figure S1 in Supplementary Material). The hydrodynamic radii and zeta potential values of bare SAMNs and of the nanohybrid were measured by dynamic light scattering (DLS) using a Zetasizer Nanoparticle analyser ZEN3600 (Malvern Instrument, UK). Both measurements were carried out with naked SAMNs and SAMN@SMOX at 50 mg/L concentration in 1 mM HEPPS pH 8.0, at room temperature. The enzyme activity was assessed following the kinetic assay described by Stevanato et al. [26]. Briefly, SMOX was incubated in the presence of 3 mM N,-N dimethyl-aniline (DMA), 4 mM 4-amineanitpyrine (AMP), 5 U/mL horseradish peroxidase (HRP), and Spm as substrate in a 20 mM HEPPS buffer at pH 8.0, at 28 °C. The hydrogen peroxide produced by the two-step reaction was continuously monitored by the change of absorbance at 544 nm, using a molar extinction coefficient (ε) of 1.25 x 10^4 $M^{-1}cm^{-1}$. Kinetic assays were performed with increasing concentrations of the substrate (from 0.01 to 1.00 mM spermine), using 5 mg/L of soluble enzyme and 0.25 g/L SAMN@SMOX. The kinetic parameters were determined according to the Michaelis-Menten model. The enzyme kinetic characterization was carried out with a VICTOR X4 2030 Multilabel Reader (Perkin Elmer, Waltham, MA, USA), with 96-wells Iwaki microplate (Asahi Techno Glass, Japan). The production of the colored dye was monitored for 1 h, initial velocity (v_0) was extrapolated in the linearity range comprised between 10 min and 25 min and plotted according to the Michaelis-Menten model. As controls, measurements in the absence of substrate were considered. Fourier transform infrared (FTIR) analysis of native enzyme, bare SAMNs, and SAMN@SMOX were performed using an IR Affinity-1S spectrometer (Shimadzu Corp., Kyoto, Japan) equipped with a diamond ATR analyzer and LabSolutions IR software (Shimadzu Corp., Kyoto, Japan). The scanning range was between 500 and 4000 cm^{-1} with a resolution of 4 cm^{-1} and 300 accumulated scans. Quantitative analysis of the native enzyme secondary structures and SAMN@SMOX hybrid was based on a curve fitting of amide I band according to Hebia and co-authors [27]. The structure content was quantified by band deconvolution using Gaussian model considering the following secondary structure motifs: β-sheet (1637–1610 cm^{-1}), random coil (1648–1638 cm^{-1}), α-helix (1660–1650 cm^{-1}), β-turn (1680–1660 cm^{-1}) and β-antiparallel (1692–1680 cm^{-1}). Circular dichroism spectra were acquired by a Jasco J-800 instrument (Jasco Int. Co., Japan) in 10 mM HEPPS, pH 8.0 in a quatx cuvette (p.l. 0.2 cm). Transmission electron microscopy (TEM) micrographs were acquired by a Jeol JEM-2010 microscope (Jeol Ltd., Tokyo, Japan) operating at 200 kV with a point-to-point resolution of 1.9 Å. Before measurements, samples were dispersed in ethanol and the suspension was treated by ultrasound for 10 min. A drop of dilute suspension was placed on a carbon-coated copper grid and allowed to dry by evaporation at room temperature.

The amino acidic sequence of SMOX was retrieved from the RCSB Protein Data Bank. Since the PDB code of mouse SMOX is not available, the crystal structure of the human SMOX was selected (PDB code: 7OXL). This is done knowing that the sequences of the two structures are equal at a 94.23% level (comparison made with the SWISS-MODEL Repository [28]). The selected PDB code was then used for the image processing with PyMOL (The PyMOL Molecular Graphics System, Version 2.0 Schrödinger, LLC).

The dependence on ionic strength (I) of kinetic parameters (k_{cat}, K_M and k_{cat}/K_M) of soluble and SAMN immobilized SMOX was studied in 10 mM HEPPS at pH 8.0 by adding 5-25 mM NaCl. The kinetic data were analysed according to the Debye-Hückel equation [29]:

$$logk = logk_0 + 2CZ_aZ_b(I)^{\frac{1}{2}} \quad (1)$$

where k is the kinetic parameter (k_{cat}, K_M and k_{cat}/K_M), Z_a and Z_b are the charges of the interacting species, k_0 is the value of the kinetic parameter at I = 0, and constant C is assumed to be 0.5 $M^{-1/2}$ at 22 °C, in water [30]. A least-squares analysis was performed with commercial graphic software (SigmaPlot 10.0 program, Jandel, Scientific). The values of the best fit parameters and the standard error of the mean value (SEM) are reported. All determinations were performed at least in triplicate.

 doi:10.20944/preprints202311.0583.v1

3. Results

3.1. Chemical-Physical Characterization of the SAMN@SMOX Hybrid

Aiming at the development of a novel biologically active nano-hybrid, a simple self-assembly approach was used for the direct interaction of SMOX with naked SAMNs. The protein strong chelating moieties, i.e. the His-tags present in the recombinant enzyme, were used to anchor SMOX to the SAMN surface according to the following rationale. At the physical boundary of maghemite nanoparticles, the crystal is interrupted and, as a consequence, the surface exposes to the milieu a distribution of iron(III) sites, which are not entirely coordinated. Ligand binding is therefore thermodynamically favored as it induces the restoration of the aforementioned dangling bonds [21]. This phenomenon is known as surface reconstruction and, generally, it is accompanied by a red-shift of the nanoparticle absorption spectrum [31]. In this view, SAMNs represent an elective paradigm, and the aforementioned red-shift emerged as a common trait in our previous studies, including the nanoparticle hybridization with proteins [32]. In Figure 1A, the integration of SMOX with SAMNs induced a red-shift of the absorption maximum of about 40 nm and the appearance of a shoulder at around 500 nm, confirming the expected coordinative nature of the SAMNs-SMOX interaction. Furthermore, the binding of SMOX onto SAMN surface was studied by adsorption isotherm models according to Giles [33] and Langmuir [34]. The binding reaction was performed in 10 mM HEPPS buffer at pH 8.0, at constant SAMN concentration (500 mg L^{-1}) and SMOX concentrations ranging from 5 to 200 mg L^{-1}, under gentle agitation for 2 h at 4 °C. In order to release loosely bound SMOX, the hybrids were magnetically separated and washed several times with the incubation buffer. In order to estimate the concentration of bound enzyme, SMOX concentration in the supernatants of the hybridization and washing steps was compared to the initial enzyme concentration. Protein quantification was carried out via spectrofluorometric measurements as described in the materials and methods section.

The Giles model [33] is a useful preliminary approach which considers the trend of the curve of the bound ligand (Q) against the free ligand in solution at the equilibrium (C_e). In Figure S2, the SAMN-SMOX system displayed a saturation behavior indicating the successful integration of the biological macromolecule to the magnetic core and prompting that once the first shell is completed, no further protein adsorption to SAMNs can occur. On these bases, the Langmuir isotherm model represents a suitable model for a more in-depth study on the development of a monomolecular core-shell system. Actually, one fundamental assumption of the Langmuir model is the formation of a single adsorbate monolayer [34]. The following linearized form of the Langmuir isotherm was adopted:

$$\frac{C_e}{Q} = \frac{1}{Q_{max} K_L} + \frac{1}{Q_{max} C_e} \quad (2)$$

where Q is the loading capacity (mg g^{-1}, namely mg protein on g nanoparticles) at a specific protein equilibrium concentration (Ce, expressed in mg L^{-1}), Q_{max} is the maximum loading capacity (expressed as mg g^{-1}), and KL is the Langmuir stability constant (expressed in mL mg^{-1}). Q_{max} and K_L were calculated from the slope and the intercept of the linear C_e/Q vs C_e plot.

Noteworthy, the Langmuir isotherm properly fitted the SMOX binding (R^2 = 0.963, Figure 1B), confirming the formation of a mono-molecular shell onto SAMN surface. The theoretical maximum loading capacity, Q_{max}, resulted of 155.8 ± 13.6 mg SMOX per g SAMNs, fully in harmony with previously reported single layer core-shell systems obtained by the direct hybridization of SAMNs with large polypeptidic molecules [22,32]. Furthermore, the calculated Langmuir constant, K_L, resulted 43.1 ± 10.4 mL/mg, again in very good agreement with stable Langmurian nano-bio-conjugates [32].

Taking in consideration the loading capacity (Q_{max}), the theoretical number of SMOX molecules per single SAMN was calculated using the following equation:

Preprints (www.preprints.org) | NOT PEER-REVIEWED | Posted: 9 November 2023 doi:10.20944/preprints202311.0583.v1

$$\frac{number\ of\ SMOX}{SAMN} = \frac{Q_{max}\ \mathrm{NA\ V}\ d_{\gamma-Fe2O3}}{M} \quad (3)$$

where NA is the Avogadro number, M is molar mass of the SMOX dimer (136 kDa, vide supra), V is the volume of a single nanoparticle, calculated by simple approximation of a SAMN to a sphere with an average diameter of 11 nm, and $d_{\gamma\text{-}Fe2O3}$ is the density of maghemite (4.8 g cm^3). The product of the last two terms is the mass of a single SAMN. The ratio resulted 2.4, hence it can be concluded that a monolayer could likely comprise from 2 to 3 enzyme molecules per nanoparticle.

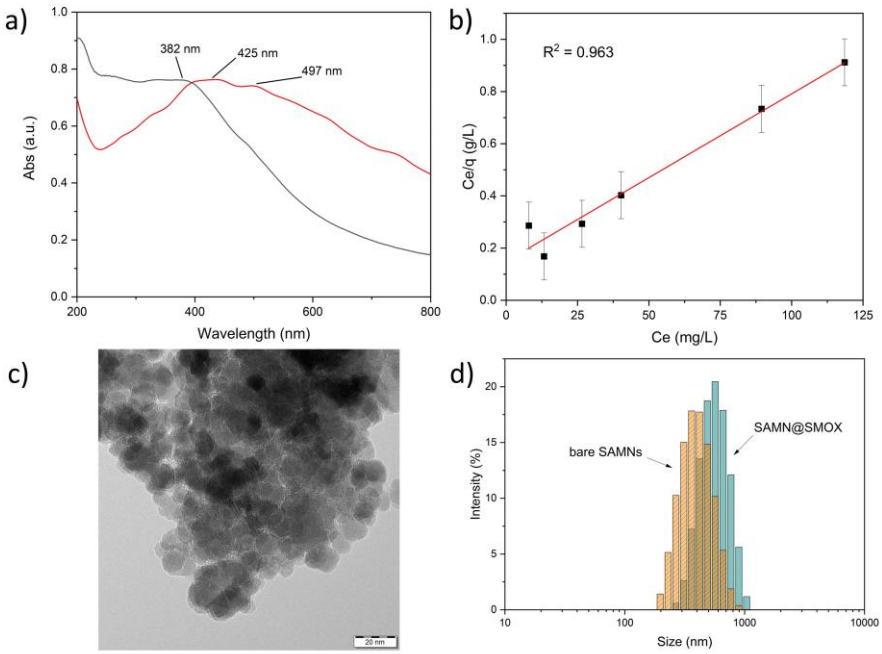

Figure 1. chemical-physical and morphological characterization of SAMN@SMOX. Comparison of the UV-Vis spectra of naked SAMNs (black line) and SAMN@SMOX (a) linearized Langmuir isotherm of the SMOX binding onto SAMNs. (b) Linear Langmuir model. (c) TEM analyses of the SAMN@SMOX. (d) DLS measurements with the statistical fitting according to the LogNorm function, orange bars for bare SAMNs and blue bars for SAMN@SMOX.

The morphological and hydrodynamic features of SAMN@SMOX were examined using transmission electron microscopy (TEM) and dynamic light scattering (see Materials and Methods section). TEM micrographs of SAMN@SMOX (Figure 1c) witnessed the formation of core-shell hybrids constituted of a single, well-preserved magnetic core embedded into a less electron dense organic envelop. However, the relatively contained thickness of the carbonaceous phase, measuring around 2 nm, can be ascribed to the TEM sample preparation. Furthermore, the zeta potential (ζ) measurements were carried out and, under the current conditions (see Materials and Methods), the ζ value of bare nanoparticles resulted +6.7 ± 1.6 mV (conductivity = 0.072 mS/cm at 25°C). The remarkable colloidal stability of water suspensions of SAMNs was extensively commented in several previous publications and it is mirrored by an extremely high ζ for a naked iron oxide nanoparticles, standing well above +30.0 mV. The here registered low zeta potential value can be likely attributed to the pH of the medium used for the analysis (pH = 8.0). Noteworthy, the ζ value of SAMN@SMOX was −19.7 ± 0.5 mV (conductivity = 0.057 mS/cm at 25 °C). It should be considered that an aqueous suspension of a nanomaterial possessing a ζ comprised in the 20–30 mV range can be classified as stable, for either positive or negative values. The latter is a suitable characteristic for future in vitro and in vivo investigations. The analysis of the hydrodynamic radii is reported in Figure 1d. For unmodified SAMNs, the hydrodynamic size resulted of 432.6 ± 56.9 nm, exceptionally large in comparison that measured in water suspension (Figure 1d, orange bars). Again, this can be ascribed to the aggregation processes at the pH of the milieu employed in the self-assembly reaction and used

Preprints (www.preprints.org) | NOT PEER-REVIEWED | Posted: 9 November 2023 doi:10.20944/preprints202311.0583.v1

in the DLS analysis. SAMN@SMOX showed a hydrodynamic diameter of 787.7 ± 48.3 nm (Figure 1d, blue bars). The magnitude of the measured hydrodynamic radius is comparable with previously reported core-shell nanostructure constituted by a single SAMN core and a protein mono-molecular layer [22].

Fourier transform infrared spectroscopy (FTIR) was used for investigating the occurrence of possible structural alterations of the enzyme upon direct immobilization on SAMN surface. As visible in Figure 2a, the SAMN@SMOX complex evidence two main bands at 1645 and 1540 cm^{-1} corresponding to SMOX amide-I and amide-II bands, thus confirming the successful immobilization of the enzyme. All the other observable bands in the FTIR profile of the SAMN@SMOX complex can be ascribed to the nanoparticle core. In particular, the peaks at 550, 630 and 690 cm^{-1} are the Fe-O stretching vibrations while the 3420 cm^{-1} refer to OH stretching.

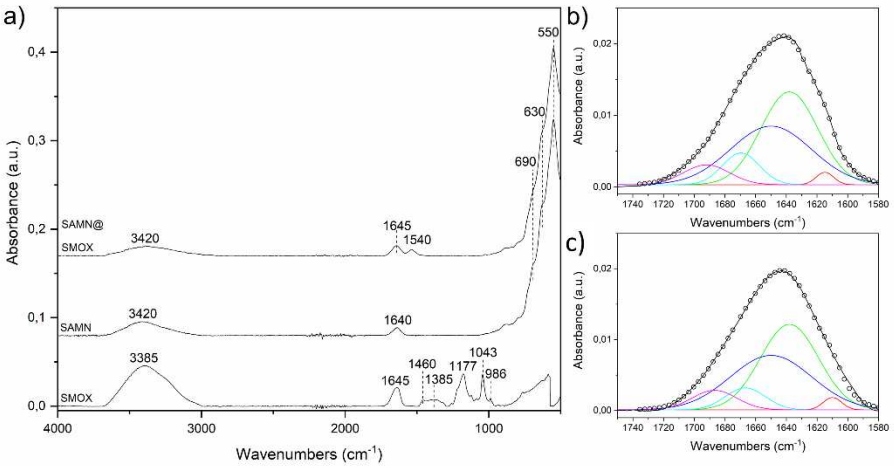

d)

Secondary structure	β-sheets	random coil	α-helix	β-turn	β-antiparallel	R^2
	%	%	%	%	%	%
SMOX	1.770	42.872	38.401	9.551	7.405	0.998
SAMN@SMOX	2.044	43.761	38.889	7.681	7.625	0.996

Figure 2. a) FT-IR spectra of SMOX, naked SAMNs and SAMN@SMOX complex. b, c) Deconvolution of amide-I band of SMOX and SAMN@SMOX complex respectively. Experimental amide-I band (black line), gaussian fitting curve (black dots), β-sheet (red line), random coil (green line), α-helix (blue line), β-turn (light blue line) and β-antiparallel (purple line). d) Secondary structure contents of native SMOX and of the SAMN@SMOX hybrid according to the deconvolution of the FTIR amide-I band.

Interestingly, the amide-I band of SMOX did not experience a shift in position neither a visible change in the shape upon binding, thus suggesting a preservation of the structure of the native enzyme. In order to deeply investigate the secondary structure conformation of SMOX and quantify even negligible structural changes upon binding the amide-I band was subjected to deconvolution (Figure 2b and c). The contribution of all the structural components obtained by the analysis are reported in Figure 2d. The deconvolution clearly shows that the interaction between SMOX and SAMNs slightly affected the enzyme structure. The whole structural components highlight changes in the range of 0.2-2% thus suggesting that the enzyme resulted unaffected upon the complexation.

In order to shed more light into possible structural modification of SMOX upon immobilization on SAMNs, both enzyme forms were characterized by circular dichroism (CD). The CD spectrum of parent SMOX showed a positive peak at 195 nm and a negative broad band, approximately centered at 220 nm, common in proteins (Figure 3, red line) [35]. The same features were observed in the CD spectrum of the SAMN@SMOX hybrid (Figure 3, blue line), providing additional evidence of the self-assembly of the SAMN@SMOX nano-bio-conjugate, as well as of the preservation of the overall

Preprints (www.preprints.org) | NOT PEER-REVIEWED | Posted: 9 November 2023 doi:10.20944/preprints202311.0583.v1

structure of the native enzyme. It is worth mentioning that based on the author's knowledge even minor conformational changes can result in drastic modifications of the catalytic behavior [22].

a)

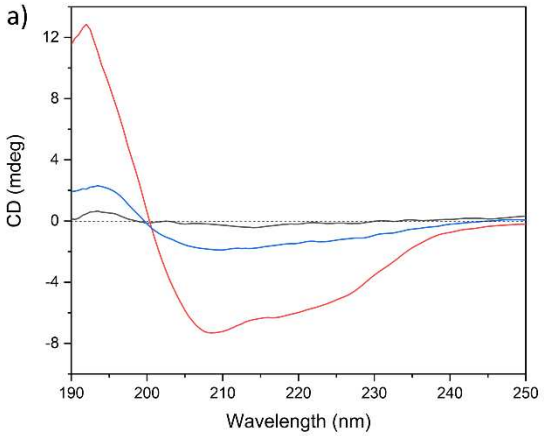

b)

Secondary structure	SMOX	SAMN@SMOX
Helix	38.4%	38.2%
Antiparallel	8.6%	5.4%
Parallel	1.0%	6.6%
Turn	11.2%	10.5%
Others	40.8%	39.4%

Figure 3. a) Circular dichroism spectra of SMOX (red, 1.1 μM), naked SAMNs (black, 0.5 g/L) and SAMN@SMOX (blue, 0.5 g/L) in 10 mM HEPPS at pH 8.0. b) Secondary structure contents of native SMOX and of the SAMN@SMOX hybrid according to circular dichroism.

3.2. Comparison of the Activity of Native SMOX and of SAMN@SMOX Hybrid

Kinetic parameters (i.e., K_M, k_{cat} and k_{cat}/K_M) of native and nano-immobilized SMOX were determined by the spectrophotometric assay described by Stevanato et al [26] and compared according to Michaelis-Menten model in Figure 4a and b, and the kinetic parameters obtained are reported in Figure 4c.

a)

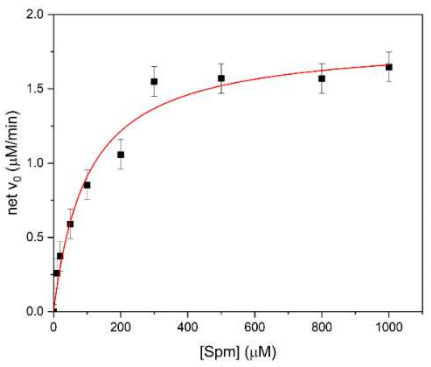

b)

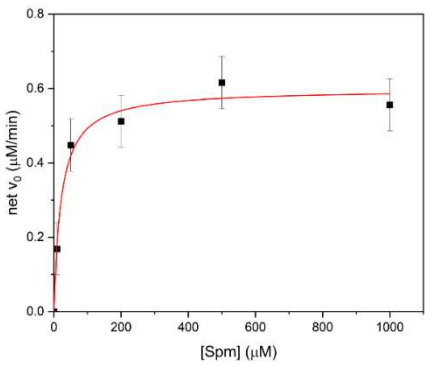

c)

Enzyme form	K_M (μM)	k_{cat} (min^{-1})	k_{cat}/K_M (M^{-1} min^{-1} x 10^{-4})
Native SMOX	108 ± 25	6.3 ± 0.6	5.8
SAMN@SMOX	29 ± 11	1.7 ± 0.2	5.8

Figure 4. Kinetic study of the native SMOX and of SAMN@SMOX. Michaelis-Menten curves of native SMOX (a) and of SAMN@SMOX (b); c) kinetic parameters of SMOX and of SAMN@SMOX.

Noteworthy, the Michaelis-Menten constant showed a significant decrease upon SMOX nano-immobilization. This is not a trivial outcome, revealing an enhancement of the affinity of the immobilized SMOX for spermine. Differently, the k_{cat} value showed by the SAMN@SMOX hybrid, even if lower than that of the native enzyme, indicates that naked SAMNs discloses a favorable local environment for enzyme harboring. Interestingly, the catalytic efficiency (k_{cat}/K_M) did not change

Preprints (www.preprints.org) | NOT PEER-REVIEWED | Posted: 9 November 2023 doi:10.20944/preprints202311.0583.v1

upon immobilization, indicating that the activity of SMOX, at low substrate concentration, was not affected by SAMNs. This result suggests a feasibility of the application of the SAMN@SMOX hydrid in terms of preservation of enzyme activity under physiologic conditions.

Previous studies [9,36] showed that the SMOX active site contains polar residues (Ser527, Tyr482, Gln200, His82 and Glu224) which play a key role in the SPM-SMOX interaction. In particular, these residues are involved in the positioning of the substrate into the active site by electrostatic/polar interaction (such as between the Glu224 and the positively charged N14 of SPM), affecting consequently also the rate of the chemical step (represented by the catalytic constant). Thus, to obtain information on electrostatic interactions involved in the activity of soluble and SAMN immobilized SMOX, and most importantly on the effect of the iron oxide nanoparticle on the substrate recognition and oxidation by the immobilized enzyme, the dependence of the kinetic parameters k_{cat}/K_M, k_{cat} and $1/K_M$ on ionic strength (I) was studied, using spermine as substrate. The K_M value, according to the Michaelis Menten model, is defined by the contribution of different kinetic constants, including k_{cat} [37], and, under particular conditions, it represents the dissociation constant of the substrate–enzyme complex. Consequently, to evaluate the effect on the association constant of the SMOX-SPM complex, the $1/K_M$ values should be considered. Measurements were carried out at pH 8.0, and at this pH value the calculated electrical charge of spermine is +3.34 [38], see Figure 5.

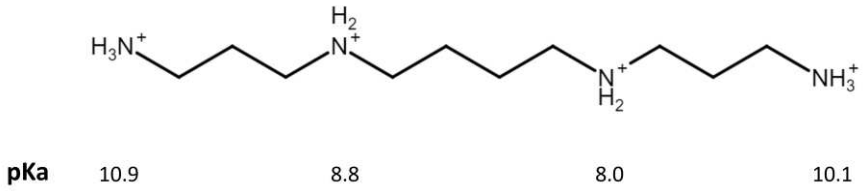

Figure 5. Spermine chemical structure. In evidence the four amino groups and the corresponding pKa values used for calculating the electrical charge of the polyamine [38].

Moreover, differently to previous kinetic characterization of SMOX [36], measurements were carried out in 10 mM HEPPS at pH 8.0 ($I = 5 \times 10^{-3}$ M) [39], and ionic strength was varied by the addition of NaCl (5-25 mM). Results were analyzed according to the Debye-Hückel equation [29] as described in Methods. The plots of $\log(k_{cat})$ vs. $I^{1/2}$, $\log(1/K_M)$ vs. $I^{1/2}$ and $\log(k_{cat}/K_M)$ vs. $I^{1/2}$ of SMOX and SAMN@SMOX showed roughly linear dependences, indicating an important role of electrostatic interactions in the recognition and in the catalytic steps of both enzyme forms (Figure S3). Indeed, from the slopes of the above mentioned plots ($2C \cdot Z_{enz} \cdot Z_{sub}$) reported in Table 1, it is possible to estimate the product of interacting charges ($Z_{enz} \cdot Z_{sub}$) during enzyme activity on spermine, being the 2C factor of eqn 1 approximately equal to 1.

As regards soluble SMOX, a strongly negative value of the slope of the $\log(k_{cat})$ vs the square root of ionic strength plot was found ($2C \cdot Z_{enz} \cdot Z_{sub} \approx -5.6$), indicating that the rate of the catalytic steps depend on interaction of opposite charges, and, considered the charge of spermine ($Z_{sub} = +3.34$), the enzyme should contribute with about 2 negatively charge residues, in agreement with previous studies [36]. Differently, in the case of SAMN@SMOX on spermine, the dependence of the catalytic constant on $I^{1/2}$ showed a lower value of interacting charges product ($2C \cdot Z_{enz} \cdot Z_{sub} \approx -1.6$). Possibly, the slight modification of enzyme structure upon immobilization on SAMNs observed by circular dichroism affected the catalytic steps (k_{cat} of soluble enzyme is higher than that of the immobilized SMOX) changing the role played by the electrostatic interactions.

Preprints (www.preprints.org) | NOT PEER-REVIEWED | Posted: 9 November 2023 doi:10.20944/preprints202311.0583.v1

Table 1. Slopes of the log(k_{cat}) vs. $I^{1/2}$, log(K_M) vs. $I^{1/2}$ and log(k_{cat}/K_M) vs. $I^{1/2}$ (that is $2C \cdot Z_{enz} \cdot Z_{sub}$ products) of native SMOX and SAMN@SMOX, where k_{cat} is the catalytic constant, K_M is the Michaelis-Menten constant and the k_{cat}/K_M ratio is the catalytic efficiency.

	$2C \cdot Z_{enz} \cdot Z_{sub}$		
	k_{cat}	k_{cat}/K_M	$1/K_M$
Native SMOX	-5.6	+1.9	+7.7
SAMN@SMOX	-1.6	-5.9	-3.9

As regards the slope of the log($1/K_M$) vs $I^{1/2}$ plot of the soluble SMOX, its positive values ($2C \cdot Z_{enz} \cdot Z_{sub} \approx +7.7$), suggests the involvement of about 2 positive charges in the enzyme active site in the control of the substrate-active site recognition process. Differently, in the case of SAMN@SMOX hybrid the $2C \cdot Z_{enz} \cdot Z_{sub}$ product was negative ($2C \cdot Z_{enz} \cdot Z_{sub} \approx -3.9$), indicating an important reduction of enzyme affinity for spermine with increasing ionic strength. This effect can be attributed to the reduction of the electrostatic attraction between the positively charged substrate and the nanoparticle immobilized SMOX (zeta potential, $\zeta = -19.7 \pm 0.5$ mV) produced by the increasing electrolyte concentration. Finally, the effect of ionic strength on the catalytic efficiency (k_{cat}/K_M) of SMOX and SAMN@SMOX was considered. The k_{cat}/K_M parameter represents the apparent second order kinetic constant of the enzyme substrate reaction, namely the kinetic constant defining the enzyme activity at low substrate concentration ([S] << K_M). The calculated $2C \cdot Z_{enz} \cdot Z_{sub}$ product corresponding to the slope of the log (k_{cat}/K_M) vs. $I^{1/2}$ was ≈ + 1.9 in the case of soluble SMOX and ≈ - 5.9 for the SAMN@SMOX hybrid. Considering that at low ionic strength ($I = 5 \times 10^{-3}$ M in 10 mM HEPPS at pH 8.0) the catalytic efficiency (k_{cat}/K_M) of SMOX and SAMN@SMOX assumed identical values (see Figure 4c), enzyme binding to nanoparticles drastically modified the electrostatic interactions between SMOX and its substrate. The reduction of the k_{cat}/K_M kinetic constant with ionic strength can be interpreted as the shielding of electrostatic attraction between SAMN@SMOX (zeta potential, ζ value of SAMN@SMOX = -19.7 ± 0.5 mV) and spermine as substrate ($Z_{sub} = +3.34$).

Computational simulations of interfaces are widely considered as reliable methods to understand nanomaterial-biomolecule interactions [40]. Herein, in order to identify the macromolecule region used by SMOX for spontaneously anchoring onto SAMN surface and its spatial positioning in the SAMN@SMOX hybrid, molecular simulations using a protein representation software were performed. Actually, the steric orientation is of fundamental importance for the availability of the enzyme active site. The crystal structure of SMOX (PDB code: 7OXL) was obtained from Protein Data Bank and processed using PyMOL (see Materials and Methods). The recombinant protein exposes the His-tag moieties on the opposite side with respect to the catalytic site, namely at the C-terminus [41]. In this view, it is important to recall the strength of His-tag groups as Fe^{3+} chelators, making the C-terminus an elective side for the docking of SMOX onto nanoparticle surface. As reported elsewhere, proteins displaying readily interacting regions do not need to adapt their structure for maximizing the contact with nanoparticles [21]. This fact plausibly explains the preservation of SMOX three-dimensional structure, which is necessary but not sufficient requisite for the enzyme to exert its biological activity. In Figure 6a, the 3D conformation of SMOX can be observed as well as a pictorial representation of its interaction with SAMNs. Noteworthy, the latter would force the protein to expose the catalytic site to the milieu, which represents a mandatory condition for substrate recognition. Finally, the negative nano-environment generated by the hybrid likely influences the electrostatic interactions between the charged amino-acid in the catalytic pocket and the substrate (Figure 6b).

Preprints (www.preprints.org) | NOT PEER-REVIEWED | Posted: 9 November 2023 doi:10.20944/preprints202311.0583.v1

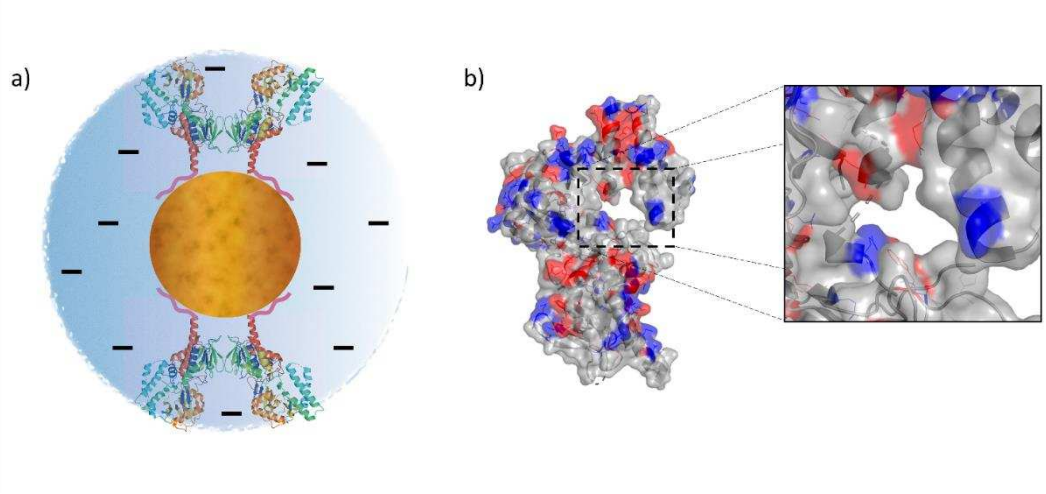

Figure 6. a) Pictorial representation of SMOX-SAMN interaction with the computation model of the protein (represented as alfa, beta and random-coil structures) bridged to the nanoparticle (orange sphere) surface by exemplified His-tag moieties (pink-colored tails). b) The N-terminus side pointing the solvent. Inset: the exposed catalytic cleft.

4. Discussion

The use of enzymes as drugs is hampered by several factors, including the possible loss of catalytic activity and low bioavailability. Despite the well-known risk related to enzyme binding to solid surfaces, enzyme–nanomaterial hybridization is believed to have real chances to overcome these limitations. Most importantly, there is an increasing consciousness that the proper enzyme-nanoparticle combination can also lead to unpredictable novel biological features that can be strategically employed in real world scenarios. In the present work, SMOX was hybridized with peculiar iron oxide nanoparticles, merging supermagnetism and intrinsic fluorescence with unique colloidal stability. Indeed, the as-obtained SAMN@SMOX nanohybrid represents an interesting example of the possible modulation of the functions of an enzyme due to the protein-nanoparticle coupling, ideally leading to a pseudo-novel biological entity. Noteworthy, besides showing a slightly reduced catalytic activity in comparison to the native enzyme, the bioactive cargo revealed an own distinctive behavior related to its response to ionic strength. In this view, soluble SMOX was subjected for the first time to an extensive kinetic characterization in an interval of medium salinity ranging from 5 to 25 mM NaCl, enlightening that SMOX-Spermine interplay is ruled by electrostatic interactions. These interactions, when the enzyme is in its nano-immobilized form, are influenced by the ionic strength in a completely different manner. To summarize, the main results on the effect of ionic strength evidenced that the physical interactions in the SMOX active site are affected by ionic strength involving positive charges of SPM and of soluble SMOX. On the other hand, when the enzyme is immobilized on nanoparticles, the presence of SAMN surface and of a slight SMOX structural modification determine a modification of the effect of electrostatic interactions between the enzyme and its substrate. In this case, the interactions involve positive charges of SPM and negatively charged nano-environment generated by SAMN@SMOX (vide supra), significantly improving the substrate-enzyme recognition steps.

5. Conclusions

SMOX has a great importance for its involvement in the polyamine catabolic pathway and, due to its biological function, can be strategically employed in enzyme therapy. The present work, besides suggesting the feasibility of the application of the SAMN@SMOX hybrid in terms of preservation of enzyme activity under physiologic conditions, encourages the nascent awareness about the often-unpredictable benefits derived by enzyme–nanoparticle hybridization. In particular, minor structural

modifications of the enzymatic cargo and of the nano-environment that SAMN@SMOX hybrid exposes to the solvent emerged as potential key factors for the modulation of SMOX function.

Supplementary Materials: The following supporting information can be downloaded at the website of this paper posted on Preprints.org. Figure S1: Fluorescence calibration curve of the enzyme spermine oxidase in 10 mM HEPPS pH 8, Figure S2: Giles isotherm of the SMOX binding onto SAMNs, Figure S3: Dependence of kinetic parameters of soluble SMOX and SAMN@SMOX on ionic strength.

Author Contributions: G.R.; investigation, formal analysis, data curation, visualization, supervision, M.M., conceptualization, writing—original draft preparation, review and editing, supervision, F.T.; Software, Methodology, A.C.; writing—review and editing, supervision; L.R.; investigation; A.C.; investigation, data curation, visualization, S.M.; investigation, data curation, visualization; M.L.D.P.; data curation, formal analysis; writing—review and editing; C.F.., investigation; MNR, investigation, writing—review and editing; M.C.; writing—review and editing; F.V., resources, writing—review and editing, project administration.

Funding: Alessandro Cecconello was supported by REACT-EU PON "Ricerca e Innovazione 2014–2020". Federica Tonolo was supported by "iNEST- Interconnected Nord-Est Innovation ECS00000043". Aura Cencini was supported by the Italian Ministry of Education, University and research (MIUR) funds "Sentinel" and "Ecosistema dell'Innovazione". Manuela Cervelli was supported by the National Funding for Centers of Excellence (Science Department 2023–2027, Roma Tre University, MIUR, Articolo 1, Commi 314–337, Legge 232/2016).

Institutional Review Board Statement: Not applicable.

Informed Consent Statement: Not applicable.

Acknowledgments: All authors gratefully acknowledge Jana Stráská of the Czech Advanced Technology and Research Institute (Catrin. Olomouc Czech Republic) for the electron microscopy images.

Conflicts of Interest: The authors declare no conflict of interest.

References

1. Polticelli, F.; Salvi, D.; Mariottini, P.; Amendola, R.; Cervelli, M. Molecular Evolution of the Polyamine Oxidase Gene Family in Metazoa. *BMC Evol. Biol.* **2012**, *12*, 1–14, doi:10.1186/1471-2148-12-90.
2. Mastrantonio, R.; Cervelli, M.; Pietropaoli, S.; Mariottini, P.; Colasanti, M.; Persichini, T. HIV-Tat Induces the Nrf2/ARE Pathway through NMDA Receptor-Elicited Spermine Oxidase Activation in Human Neuroblastoma Cells. *PLoS One* **2016**, *11*, e0149802, doi:10.1371/journal.pone.0149802.
3. Ceci, R.; Duranti, G.; Leonetti, A.; Pietropaoli, S.; Spinozzi, F.; Marcocci, L.; Amendola, R.; Cecconi, F.; Sabatini, S.; Mariottini, P.; et al. Adaptive Responses of Heart and Skeletal Muscle to Spermine Oxidase Overexpression: Evaluation of a New Transgenic Mouse Model. *Free Radic. Biol. Med.* **2017**, *103*, 216–225, doi:10.1016/j.freeradbiomed.2016.12.040.
4. Agostinelli, E.; Belli, F.; Dalla Vedova, L.; Marra, M.; Crateri, P.; Arancia, G. Hyperthermia Enhances Cytotoxicity of Amine Oxidase and Spermine on Drug-Resistant LoVo Colon Adenocarcinoma Cells. *Int. J. Oncol.* **2006**, *28*, 1543–1553, doi:10.3892/ijo.28.6.1543.
5. Agostinelli, E.; Vianello, F.; Magliulo, G.; Thomas, T.; Thomas, T.J. Nanoparticle Strategies for Cancer Therapeutics: Nucleic Acids, Polyamines, Bovine Serum Amine Oxidase and Iron Oxide Nanoparticles (Review). *Int. J. Oncol.* **2015**, *46*, 5–16, doi:10.3892/ijo.2014.2706.
6. Ohkubo, S.; Mancinelli, R.; Miglietta, S.; Cona, A.; Angelini, R.; Canettieri, G.; Spandidos, D.A.; Gaudio, E.; Agostinelli, E. Maize Polyamine Oxidase in the Presence of Spermine/Spermidine Induces the Apoptosis of LoVo Human Colon Adenocarcinoma Cells. *Int. J. Oncol.* **2019**, *54*, 2080–2094, doi:10.3892/ijo.2019.4780.
7. Cervelli, M.; Amendola, R.; Polticelli, F.; Mariottini, P. Spermine Oxidase: Ten Years After. *Amino Acids* **2012**, *42*, 441–450, doi:10.1007/s00726-011-1014-z.
8. Cervelli, M.; Bellavia, G.; D'Amelio, M.; Cavallucci, V.; Moreno, S.; Berger, J.; Nardacci, R.; Marcoli, M.; Maura, G.; Piacentini, M.; et al. A New Transgenic Mouse Model for Studying the Neurotoxicity of Spermine Oxidase Dosage in the Response to Excitotoxic Injury. *PLoS One* **2013**, *8*, e64810, doi:10.1371/journal.pone.0064810.
9. Cervelli, M.; Angelucci, E.; Stano, P.; Leboffe, L.; Federico, R.; Antonini, G.; Mariottini, P.; Polticelli, F. The Glu216/Ser218 Pocket Is a Major Determinant of Spermine Oxidase Substrate Specificity. *Biochem. J.* **2014**, *461*, 453–459, doi:10.1042/BJ20140305.

10. Cervetto, C.; Vergani, L.; Passalacqua, M.; Ragazzoni, M.; Venturini, A.; Cecconi, F.; Berretta, N.; Mercuri, N.; D'Amelio, M.; Maura, G.; et al. Astrocyte-Dependent Vulnerability to Excitotoxicity in Spermine Oxidase-Overexpressing Mouse. *NeuroMolecular Med.* **2016**, *18*, 50–68, doi:10.1007/s12017-015-8377-3.
11. de la Fuente, M.; Lombardero, L.; Gómez-González, A.; Solari, C.; Angulo-barturen, I.; Acera, A.; Vecino, E.; Astigarraga, E.; Barreda-gómez, G. Enzyme Therapy: Current Challenges and Future Perspectives. *Int. J. Mol. Sci.* **2021**, *22*, 9181, doi:10.3390/ijms22179181.
12. Magro, M.; Venerando, A.; Macone, A.; Canettieri, G.; Agostinelli, E.; Vianello, F. Nanotechnology-Based Strategies to Develop New Anticancer Therapies. *Biomolecules* **2020**, *10*, 735, doi:10.3390/biom10050735.
13. Magro, M.; Vianello, F. Bare Iron Oxide Nanoparticles: Surface Tunability for Biomedical, Sensing and Environmental Applications. *Nanomaterials* **2019**, *9*, 1608, doi:10.3390/nano9111608.
14. Mahmoudi, M.; Lynch, I.; Ejtehadi, M.R.; Monopoli, M.P.; Bombelli, F.B.; Laurent, S. Protein-Nanoparticle Interactions: Opportunities and Challenges. *Chem. Rev.* **2011**, *111*, 5610–5637, doi:10.1021/cr100440g.
15. Niemirowicz, K.; Markiewicz, K.H.; Wilczewska, A.Z.; Car, H. Magnetic Nanoparticles as New Diagnostic Tools in Medicine. *Adv. Med. Sci.* **2012**, *57*, 196–207, doi:https://doi.org/10.2478/v10039-012-0031-9.
16. Lynch, I.; Dawson, K.A. Protein-Nanoparticle Interactions. *Nano Today* **2008**, *3*, 40–47, doi:10.1016/S1748-0132(08)70014-8.
17. Johnson, B.J.; Russ Algar, W.; Malanoski, A.P.; Ancona, M.G.; Medintz, I.L. Understanding Enzymatic Acceleration at Nanoparticle Interfaces: Approaches and Challenges. *Nano Today* **2014**, *9*, 102–131, doi:10.1016/j.nantod.2014.02.005.
18. Ding, S.; Cargill, A.A.; Medintz, I.L.; Claussen, J.C. Increasing the Activity of Immobilized Enzymes with Nanoparticle Conjugation. *Curr. Opin. Biotechnol.* **2015**, *34*, 242–250, doi:10.1016/j.copbio.2015.04.005.
19. Johnson, P.A.; Park, H.J.; Driscoll, A.J. Enzyme Nanoparticle Fabrication: Magnetic Nanoparticle Synthesis and Enzyme Immobilization. *Methods Mol. Biol.* **2011**, *679*, 183–191, doi:10.1007/978-1-60761-895-9_15.
20. Rodrigues, R.C.; Ortiz, C.; Berenguer-Murcia, Á.; Torres, R.; Fernández-Lafuente, R. Modifying Enzyme Activity and Selectivity by Immobilization. *Chem. Soc. Rev.* **2013**, *42*, 6290–6307, doi:10.1039/c2cs35231a.
21. Magro, M.; Cozza, G.; Molinari, S.; Venerando, A.; Baratella, D.; Miotto, G.; Zennaro, L.; Rossetto, M.; Frömmel, J.; Kopečná, M.; et al. Role of Carboxylic Group Pattern on Protein Surface in the Recognition of Iron Oxide Nanoparticles: A Key for Protein Corona Formation. *Int. J. Biol. Macromol.* **2020**, *164*, 1715–1728, doi:10.1016/j.ijbiomac.2020.07.295.
22. Rilievo, G.; Cecconello, A.; Molinari, S.; Venerando, A.; Rutigliano, L.; Govardhan, G.T.; Kariyawasam, D.H.; Arusei, R.J.; Zennaro, L.; Di Paolo, M.L.; et al. Acidic Shift of Optimum PH of Bovine Serum Amine Oxidase upon Immobilization onto Nanostructured Ferric Tannates. *Int. J. Mol. Sci.* **2022**, *23*, 12172, doi:10.3390/ijms232012172.
23. Zanin, S.; Molinari, S.; Cozza, G.; Magro, M.; Fedele, G.; Vianello, F.; Venerando, A. Intracellular Protein Kinase CK2 Inhibition by Ferulic Acid-Based Trimodal Nanodevice. *Int. J. Biol. Macromol.* **2020**, *165*, 701–712, doi:10.1016/j.ijbiomac.2020.09.207.
24. Cervelli, M.; Polticelli, F.; Federico, R.; Mariottini, P. Heterologous Expression and Characterization of Mouse Spermine Oxidase. *J. Biol. Chem.* **2003**, *278*, 5271–5276, doi:10.1074/jbc.M207888200.
25. Magro, M.; Sinigaglia, G.; Nodari, L.; Tucek, J.; Polakova, K.; Marusak, Z.; Cardillo, S.; Salviulo, G.; Russo, U.; Stevanato, R.; et al. Charge Binding of Rhodamine Derivative to OH- Stabilized Nanomaghemite: Universal Nanocarrier for Construction of Magnetofluorescent Biosensors. *Acta Biomater.* **2012**, *8*, 2068–2076, doi:10.1016/j.actbio.2012.02.005.
26. Stevanato, R.; Mondovi', B.; Sabatini, S.; Rigo, A. Spectrophotometric Assay for Total Polyamines by Immobilized Amine Oxidases. *Anal. Chim. Acta* **1990**, *237*, 391–397, doi:10.1016/S0003-2670(00)83942-2.
27. Hebia, C.; Bekale, L.; Chanphai, P.; Agbebavi, J.; Tajmir-Riahi, H.A. Trypsin Inhibitor Complexes with Human and Bovine Serum Albumins: TEM and Spectroscopic Analysis. *J. Photochem. Photobiol. B Biol.* **2014**, *130*, 254–259, doi:10.1016/j.jphotobiol.2013.11.025.
28. Bienert, S.; Waterhouse, A.; De Beer, T.A.P.; Tauriello, G.; Studer, G.; Bordoli, L.; Schwede, T. The SWISS-MODEL Repository-New Features and Functionality. *Nucleic Acids Res.* **2017**, *45*, D313–D319, doi:10.1093/nar/gkw1132.
29. Atkins, P.; De Paula, J. *Atkins' Physical Chemistry*; 8th ed.; Oxford University Press: Oxford, 2006; ISBN 0198700725.
30. Butterworth, P.J. *The Chemical Kinetics of Enzyme Action (2nd Edition)*; Laidler, K.J., Bunting, P.S., Eds.; Portland Press, 1974; Vol. 2;.

31. Rajh, T.; Chen, L.X.; Lukas, K.; Liu, T.; Thurnauer, M.C.; Tiede, D.M. Surface Restructuring of Nanoparticles: An Efficient Route for Ligand-Metal Oxide Crosstalk. *J. Phys. Chem. B* **2002**, *106*, 10543–10552, doi:10.1021/jp021235v.
32. Magro, M.; Faralli, A.; Baratella, D.; Bertipaglia, I.; Giannetti, S.; Salviulo, G.; Zboril, R.; Vianello, F. Avidin Functionalized Maghemite Nanoparticles and Their Application for Recombinant Human Biotinyl-SERCA Purification. *Langmuir* **2012**, *28*, 15392–15401, doi:10.1021/la303148u.
33. Giles, C.H.; Smith, D.; Huitson, A. A General Treatment and Classification of the Solute Adsorption Isotherm. I. Theoretical. *J. Colloid Interface Sci.* **1974**, *47*, 755–765, doi:10.1016/0021-9797(74)90252-5.
34. Langmuir, I. The Adsorption of Gases on Plane Surfaces of Glass, Mica and Platinum. *J. Am. Chem. Soc.* **1918**, *40*, 1361–1403, doi:10.1021/ja02242a004.
35. Greenfield, N.J. Using Circular Dichroism Spectra to Estimate Protein Secondary Structure. *Nat. Protoc.* **2007**, *1*, 2876–2890, doi:10.1038/nprot.2006.202.
36. Tavladoraki, P.; Cervelli, M.; Antonangeli, F.; Minervini, G.; Stano, P.; Federico, R.; Mariottini, P.; Polticelli, F. Probing Mammalian Spermine Oxidase Enzyme–Substrate Complex through Molecular Modeling, Site-Directed Mutagenesis and Biochemical Characterization. *Amino Acids* **2011**, *40*, 1115–1126, doi:10.1007/s00726-010-0735-8.
37. Fersht, A. *Enzyme Structure and Mechanism*; 2nd ed.; W.H. Freeman & Co.: New York, 1985; ISBN 9780716716143.
38. Di Paolo, M.L.; Stevanato, R.; Corazza, A.; Vianello, F.; Lunelli, L.; Scarpa, M.; Rigo, A. Electrostatic Compared with Hydrophobic Interactions between Bovine Serum Amine Oxidase and Its Substrates. *Biochem. J.* **2003**, *371*, 549–556, doi:10.1042/BJ20021055.
39. Stellwagen, E.; Prantner, J.D.; Stellwagen, N.C. Do Zwitterions Contribute to the Ionic Strength of a Solution? *Anal. Biochem.* **2008**, *373*, 407–409, doi:10.1016/j.ab.2007.10.038.
40. Heinz, H.; Ramezani-Dakhel, H. Simulations of Inorganic-Bioorganic Interfaces to Discover New Materials: Insights, Comparisons to Experiment, Challenges, and Opportunities. *Chem. Soc. Rev.* **2016**, *45*, 412–448, doi:10.1039/c5cs00890e.
41. Cervelli, M.; Leonetti, A.; Cervoni, L.; Ohkubo, S.; Xhani, M.; Stano, P.; Federico, R.; Polticelli, F.; Mariottini, P.; Agostinelli, E. Stability of Spermine Oxidase to Thermal and Chemical Denaturation: Comparison with Bovine Serum Amine Oxidase. *Amino Acids* **2016**, *48*, 2283–2291, doi:10.1007/s00726-016-2273-5.